Chemical Science

EDGE ARTICLE

View Article Online
View Journal | View Issue

Cite this: *Chem. Sci.*, 2017, **8**, 1927

Bimodal supramolecular functionalization of carbon nanotubes triggered by covalent bond formation†

Sofía Leret,[a] Yann Pouillon,[b] Santiago Casado,[a] Cristina Navío,[a] Ángel Rubio[bc] and Emilio M. Pérez*[a]

Received 31st August 2016
Accepted 1st November 2016

DOI: 10.1039/c6sc03894h

www.rsc.org/chemicalscience

Many applications of carbon nanotubes require their chemical functionalization. Both covalent and supramolecular approaches have been extensively investigated. A less trodden path is the combination of both covalent and noncovalent chemistries, where the formation of covalent bonds triggers a particularly stable noncovalent interaction with the nanotubes. We describe a series of naphthalene diimide (NDI) bisalkene molecules that, upon mixing with single-walled carbon nanotubes (SWNTs) and Grubbs' catalyst, undergo two different reaction pathways. On one hand, they ring-close around the SWNTs to form rotaxane-like mechanically interlocked derivatives of SWNTs (MINTs). Alternatively, they oligomerize and then wrap around the SWNTs. The balance of MINTs to oligomer-wrapped SWNTs depends on the affinity of the NDI molecules for the SWNTs and the kinetics of the metathesis reactions, which can be controlled by varying the solvent. Thorough characterization of the products (TGA, TEM, AFM, Raman, UV-vis-NIR, PLE, XPS and UPS) confirms their structure and shows that each type of functionalization affects the electronic properties of the SWNTs differently.

Introduction

Single wall carbon nanotubes (SWNTs)[1,2] show a unique collection of physical properties that make them one of the most promising nanomaterials.[3] Their mechanical properties are already exploited in a variety of commercial applications,[4] and examples of advanced SWNT-based electronic devices are being developed.[5–10] The chemical modification of SWNTs can tune their properties and/or improve their processability. To this end, both covalent and supramolecular approaches have been extensively explored.[11–15] Each approach shows advantages and disadvantages that make it suitable for certain applications. The formation of covalent bonds implies higher stability and is typically used if permanent changes to the surface of the SWNTs are required.[16–18] On the other hand, noncovalent chemistry occurs under equilibrium, and offers the possibility of switching the interactions on and off in response to stimuli.[19–21]

A much less explored alternative is the combination of both covalent and noncovalent chemistries for nanotube functionalization, where the formation of covalent bonds triggers a particularly stable noncovalent interaction. Campidelli and co-workers have described the supramolecular encapsulation of SWNTs within porphyrin networks linked *in situ* through either S–S[22] or C–C[23] covalent bonds. More recently, Bao and co-workers have exploited the reversibility of imine bonds for the formation and removal of a conjugated polymer that wraps around large diameter SWNTs with extreme selectivity, allowing for their facile purification.[24]

We have introduced the mechanical bond as a new tool for the modification of SWNTs that exploits and combines the advantages of covalent and noncovalent chemistries.[25–28] Briefly, we utilized linear precursors equipped with terminal alkenes and two recognition units for SWNTs that help template the macrocyclization around the nanotubes through ring-closing metathesis (RCM). The products obtained are pseudorotaxane-like mechanically interlocked derivatives of SWNTs (MINTs).[29] Due to the use of alkene metathesis in the final clipping synthetic step, a possible competing reaction is the formation *in situ* of oligomers/polymers of the linear precursor through acyclic diene metathesis polymerization (ADMP). The oligomers could then wrap around the SWNTs forming particularly stable supramolecular associates (Fig. 1).

A series of control experiments showed that in the case of both exTTF and pyrene-based macrocycles, the fraction of

[a]*IMDEA Nanociencia, Ciudad Universitaria de Cantoblanco, C/Faraday 9, 28049, Madrid, Spain. E-mail: emilio.perez@imdea.org*

[b]*Departamento de Física de Materiales, Facultad de Químicas, UPV/EHU, San Sebastián, Spain*

[c]*Max Planck Institute for the Structure and Dynamics of Matter (MPSD), Luruper Chaussee 149, 22761 Hamburg, Germany*

† Electronic supplementary information (ESI) available: Synthetic details, characterization data and supplementary figures. See DOI: 10.1039/c6sc03894h

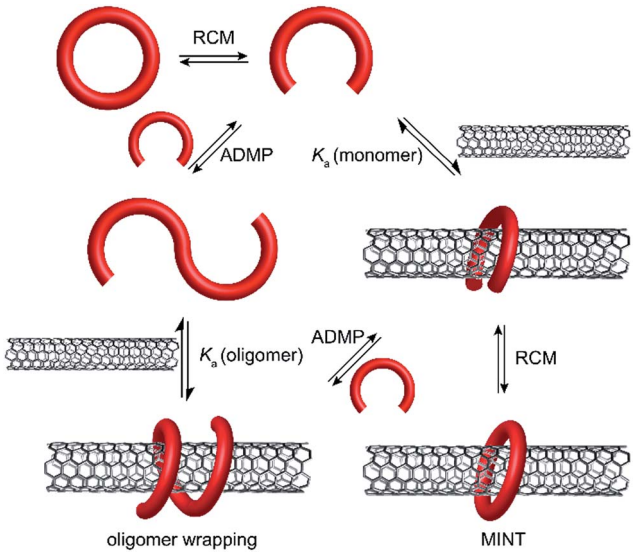

Fig. 1 Reaction pathways for the bimodal noncovalent functionalization of SWNTs to afford either oligomer-wrapped SWNTs or MINTs. Grubb's catalyst has been omitted for clarity.

SWNTs functionalized by oligomers was insignificant compared to MINTs.[25–28] However, as illustrated by the examples described above,[22–24] the formation of oligomer-wrapped SWNTs is often advantageous.

Naphthalene diimides (NDIs)[30] are part of the rylene tetracarboxylic diimides family,[31] they show remarkable photophysical properties, and are well known air-stable electron acceptor building blocks in organic electronics.[32–36] Their π-basicity has been extensively utilized in supramolecular chemistry, most notably in the emerging field of anion–π interactions,[37–40] but also in the molecular recognition of fullerenes.[41,42] Of more relevance to the present work, NDI derivatives are known to interact with SWNTs to form supramolecular hybrids.[43] With all these appealing properties in mind, we decided to explore the use of NDIs as recognition fragments in the synthesis of MINTs.

Here, we show that alkene-terminated NDI derivatives can be utilized to synthesize MINTs and oligomer-wrapped SWNTs through RCM and/or ADMP. The balance between MINTs and oligomer-wrapped nanotubes can be tuned by varying the solvent system.

Results and discussion

Design and synthesis of NDI macrocycle/oligomer precursors

The design of the NDI-based bisalkene linear precursors **1–3** is directly based on the exTTF and pyrene precedents.[25–28] The molecules feature two NDI units as recognition motifs for SWNTs, a *p*-xylylene aromatic spacer, and alkene-terminated alkyl spacers of different lengths. Solubilizing branched alkyl chains had to be added to the aromatic spacer, as the products obtained otherwise are intractable due to their insolubility. Linear precursors (**1–3**) and macrocycles (**4–6**) were synthesized as shown in Scheme 1.

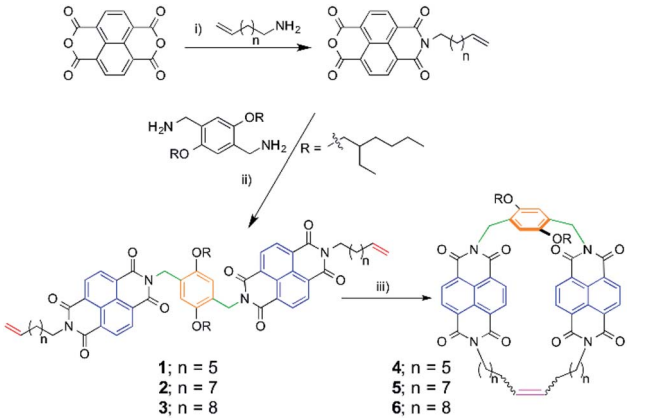

Scheme 1 Synthesis of linear precursors **1–3** and macrocycles **4–6**. Reaction conditions: (i) H_2O, 110 °C, 12 h and acetic anhydride, y = 96%; (ii) DMF, 130 °C, 5 h, y = 78%; (iii) DCM, 4 h, room temperature, y = 83%. The colour code in linear precursors and macrocycles matches that of Fig. 4 (*vide infra*).

We modelled the interaction of the macrocycles with SWNTs in MINT topology (Fig. 2A), at the Molecular Mechanics (MM) level using the MMFF94 force field, in order to accelerate the preparation of the experiments. The use of MM allows for a fast screening of candidate macrocycles, while providing a qualitatively correct description of their compatibility with the SWNTs. If the diameter of the SWNT is smaller than the cavity of the

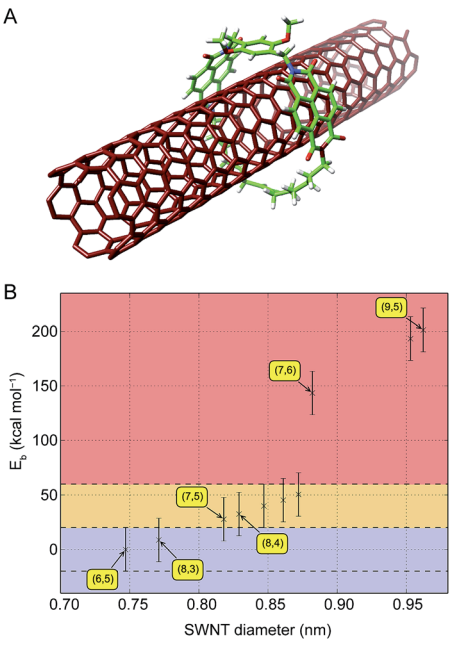

Fig. 2 (A) Energy-minimized molecular model of a MINT architecture featuring macrocycle **6** and a (6,5) SWNT. (B) Interaction energies of a series of SWNTs with macrocycle **6** (negative = attractive). Error bars of 20 kcal mol^{-1} have been represented for each combination. Blue: most favorable formation energy range. Orange: unfavourable formation energy range. Red: limit of the model. The SWNT chiralities observed experimentally have been labelled, as well as the largest diameter in the favourable area. The complete dataset is available in the ESI.†

macrocycle, their mutual interaction remains very weak and can become slightly attractive when the macrocycle closes around the nanotube, thanks to a template effect. However, when the SWNT diameter increases, internal tensions within the structure of the NDI macrocycle become relevant and make the interaction become increasingly repulsive, which would favor the formation of oligomers. As in previous examples,[25,28] we remain attentive to the quantitative limitations of this approach. In the present case, we have even increased the error bar to 20 kcal mol^{-1}, to account for the higher deviation of the force field with respect to *ab initio* calculations regarding the description of the diimide group. This larger uncertainty brings the favorable formation area below 20 kcal mol^{-1} and the validity limit of our model to 60 kcal mol^{-1}, still within range of half the intensity of a covalent C–H bond (40 kcal mol^{-1}). In addition, the flexibility of the alkyl chain – which was the key factor of compatibility for the molecules we studied previously – is partly compensated for by the rigidity of the diimides. Fig. 2B illustrates this effect when the diameter of the SWNT increases: while the interaction between the macrocycle and the nanotube smoothly increases within the validity limits of our model for small diameters, it abruptly gives way to strongly repulsive interactions above 0.88 nm. From a geometrical perspective, this corresponds to a mechanical deformation of the diimides, which is highly unfavourable to the stability of **6**. In experiments, its formation around wider nanotubes, such as (7,6) and (9,5), will thus not occur. Still, most of the chiralities present in the samples are found in the favorable diameter and energy ranges for the formation of MINTs.

Relationship of NDI loading with SWNT diameter and macrocyclic cavity

With the MM data in mind, we explored the RCM of **1–3** in the presence of (7,6)-enriched SWNTs (0.7–1.1 nm diameter, 95% purity after purification), and (6,5)-enriched SWNTs (0.7–0.9 nm diameter, 95% purity after purification), purchased from Sigma Aldrich Co. The nanotubes (5 mg) were suspended in 5 mL of either tetrachloroethane (TCE) or dimethylformamide (DMF), and mixed with the corresponding linear precursor **1–3** (0.83 mM) and Grubb's 2nd generation catalyst at room temperature for 72 hours. After this time, the suspension was filtered through a PTFE membrane of 0.2 μm pore size, and the solid washed profusely with CH_2Cl_2 to remove non-threaded macrocycles, catalyst, and any remaining linear precursor. The solid products thus obtained were analyzed through thermogravimetric analysis (TGA), affording the results summarized in Table 1.

Table 1 Degree of functionalization from TGA data (10 °C min^{-1}, air) for products of the reaction between linear precursors **1–3** and SWNTs in TCE and DMF

	1	2	3
(6,5) in TCE	19%	19%	21%
(6,5) in DMF	56%	51%	54%
(7,6) in TCE	20%	21%	23%
(7,6) in DMF	49%	48%	52%

Control experiments with preformed macrocycles **4–6** or linear precursors **1–3** without Grubbs' catalyst lead to much lower functionalization (see the ESI†). In contrast, if Grubbs' catalyst is added the reaction leads to the same products using either the macrocyclic or linear precursors, proving that the metathesis reaction is reversible under our experimental conditions.

The first observation is that the degree of functionalization in TCE is significantly lower for the NDI macrocycles than for the previously reported exTTF or pyrene macrocycles. For instance, for the product of the reaction between **1** and (6,5) SWNTs in TCE, a functionalization of 19% was observed, compared to 35% for an exTTF macrocycle with the same alkyl spacer under identical experimental conditions.[28] These results suggest a significant decrease in affinity of the NDI macrocycles for the SWNTs when compared to their exTTF counterparts, which can be accounted for by the smaller van der Waals surface of NDI and its lack of curvature, compared to exTTF.[44] Considering that it is known that the NDI–SWNT interaction is enhanced in polar solvents,[43] we attempted the MINT formation reaction in DMF, a polar solvent compatible with RCM conditions in which the nanotubes are satisfactorily dispersed. First, we measured the association constants of the monomer towards the nanotubes in both TCE and DMF at room temperature, using our previously reported method.[45] As expected, we observed a significant increase of one order of magnitude of the binding constant in the more polar DMF with respect to TCE. In particular, we measured $\log K_a = 2.6 \pm 0.1\ M^{-1}$ for **3**·(6,5) SWNTs in TCE and $\log K_a = 3.5 \pm 0.2\ M^{-1}$ for the same system in DMF (see the ESI†). This explains the larger degree of functionalization that we consistently observe in DMF, as it would favor both the formation of MINTs and of oligomer-wrapped SWNTs.

A second fact is that the degree of functionalization bears no clear dependence on the match between the diameter of the nanotubes and the size of the cavity of the macrocycles, particularly for the reactions run in DMF. For example, for the reaction of linear precursors **1**, **2**, and **3** with (7,6) SWNTs in TCE, the TGA shows 20, 21 and 23% functionalization, respectively. That is, the degree of functionalization increases with cavity size, even if only slightly.[26] However, for the same reactions in DMF, TGA analysis yields 49, 48, and 52% functionalization.

Stability of the noncovalent functionalization and kinetics of the non-templated metathesis reaction

We have previously reported that MINTs are sufficiently stable to withstand a strong thermal treatment, namely reflux in TCE (b.p. = 147 °C) for 30 min, followed by a thorough rinse with CH_2Cl_2. Under these high-temperature conditions, even particularly stable supramolecular complexes should dissociate, due to the weakening of noncovalent interactions. Indeed, when we subjected our samples to this demanding test of stability, a decrease in the degree of NDI material was observed

in all cases, in agreement with the presence of oligomer–SWNT supramolecular hybrids. Moreover, a difference between the solvents is also apparent. For the reactions run in the nonpolar TCE, the loss of NDI loading upon thermal treatment is small. For instance, for linear precursor **3**, the functionalization decreases from 23 to 19% for (7,6) SWNTs. However, for the reactions run in DMF, the loss of functionalization is much larger. Taking the same linear precursor and nanotubes for comparison, the loading goes from 52% to 38%. This is in sharp contrast with our previous findings for the exTTF-based or pyrene-based MINTs, where no significant loss of functionalization was observed.[25,26]

The large initial loading of NDI material, the lack of a clear relationship between macrocycle cavity and SWNT diameter and functionalization, and the significant loss of loading upon refluxing in TCE observed for the MINT-forming reactions run in DMF can all be understood if the participation of oligomers is significantly larger in the more polar solvent. In that case, the oligomers, which are attached to the SWNTs through non-covalent forces only, would be removed after the thermal treatment, leaving the mechanically interlocked macrocycles behind.

Persuasive experimental evidence for this hypothesis was provided by analysis of the filtrate resulting from the TCE boiling experiment. Fig. 3 displays the MALDI-TOF spectrum of the filtrate of the thermal treatment of **3**–(7,6)-DMF. Complex peaks at m/z = 2360–2479, 3529–3632, 4695–4770, and 5864–5924 correspond to the dimeric (calcd m/z = 2361), trimeric (calcd m/z = 3528), tetrameric (calcd m/z = 4695), and pentameric (calcd m/z = 5861) linear metathesis products of **3**. No signs of cyclic species were observed, proving that the MINTs do not dissociate even under these harsh conditions. Moreover, analysis of the filtrate originating from the reaction run in TCE showed no signs of oligomers.

Investigation of the metathesis reaction of **3** in the absence of template through ^{1}H NMR provided an explanation for the prevalence of oligomer-wrapped SWNTs in DMF (Fig. 4). In TCE, the reaction is very slow, and only a very small concentration of oligomers, with no significant amount of macrocycle **6**, can be found after 24 h of reaction. In contrast, in DMF, all the starting material was consumed to produce a complex mixture composed mainly of oligomers with only a small fraction of **6**. The faster reaction rate for the formation of oligomers in DMF favours the non-templated pathway depicted in Fig. 1, which can only lead to oligomer-wrapped SWNTs.

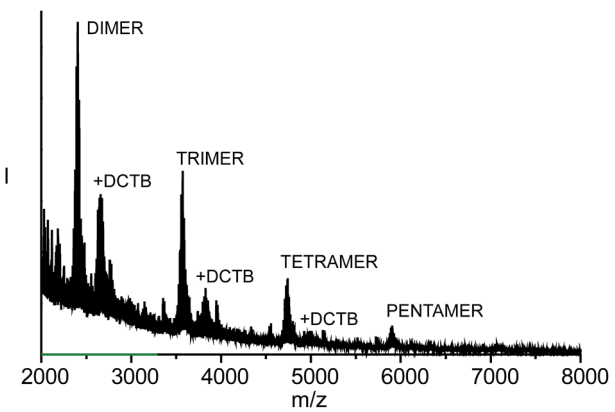

Fig. 3 MALDI-TOF spectrum (DCTB matrix) of the filtrate of the thermal treatment of the product of the reaction of **3** with (7,6) SWNTs in DMF.

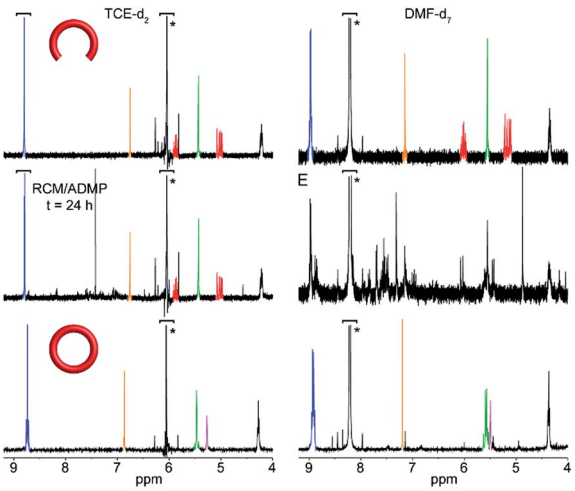

Fig. 4 Partial ^{1}H NMR (400 MHz, room temperature) of the untemplated metathesis reaction in TCE-d_2 (left panel) and DMF-d_7 (right panel). The NMRs of the linear precursor **3** and macrocycle **6** are shown for reference. Color code corresponds to the assignment as depicted in Scheme 1. Residual solvent peaks are marked with an asterisk.

TEM and AFM imaging

Investigation of the reaction products under transmission electron microscopy (TEM) and atomic force microscopy (AFM) is also consistent with the coexistence of MINT-like products and oligomer-wrapped SWNTs. For example, exploration under TEM of the product of the reaction of **3** with (6,5)-enriched SWNTs in DMF shows SWNTs with quite heavily functionalized walls (Fig. 5A). Although the material is much more sensitive to the electron beam than our previous MINT samples, which hampered correct focusing, we could observe individual circular objects of adequate size to be macrocycle **6** (*ca.* 2 nm), which are highlighted with red arrows in Fig. 5B and C. Besides that, areas of the nanotubes which are continuously modified by what appear as helical elongated molecules are also apparent, for instance that marked between two white arrows in Fig. 5B.

AFM reveals individualized SWNTs (height *ca.* 0.6 nm, odd profiles in Fig. 5D and E), which in several areas are fully covered with a dense layer of NDI material of height around 2 nm (even profiles in Fig. 5D and E), which could be either oligomer-wrapped SWNTs, or densely packed macrocycles in MINTs. Some individual macrocycles can also be seen, such as those shown in Fig. 5F.

Effects of the supramolecular functionalization on the electronic properties of the SWNTs

As we have shown, the use of TCE results in mostly MINT-type products, while the reactions run in DMF show a mixture of

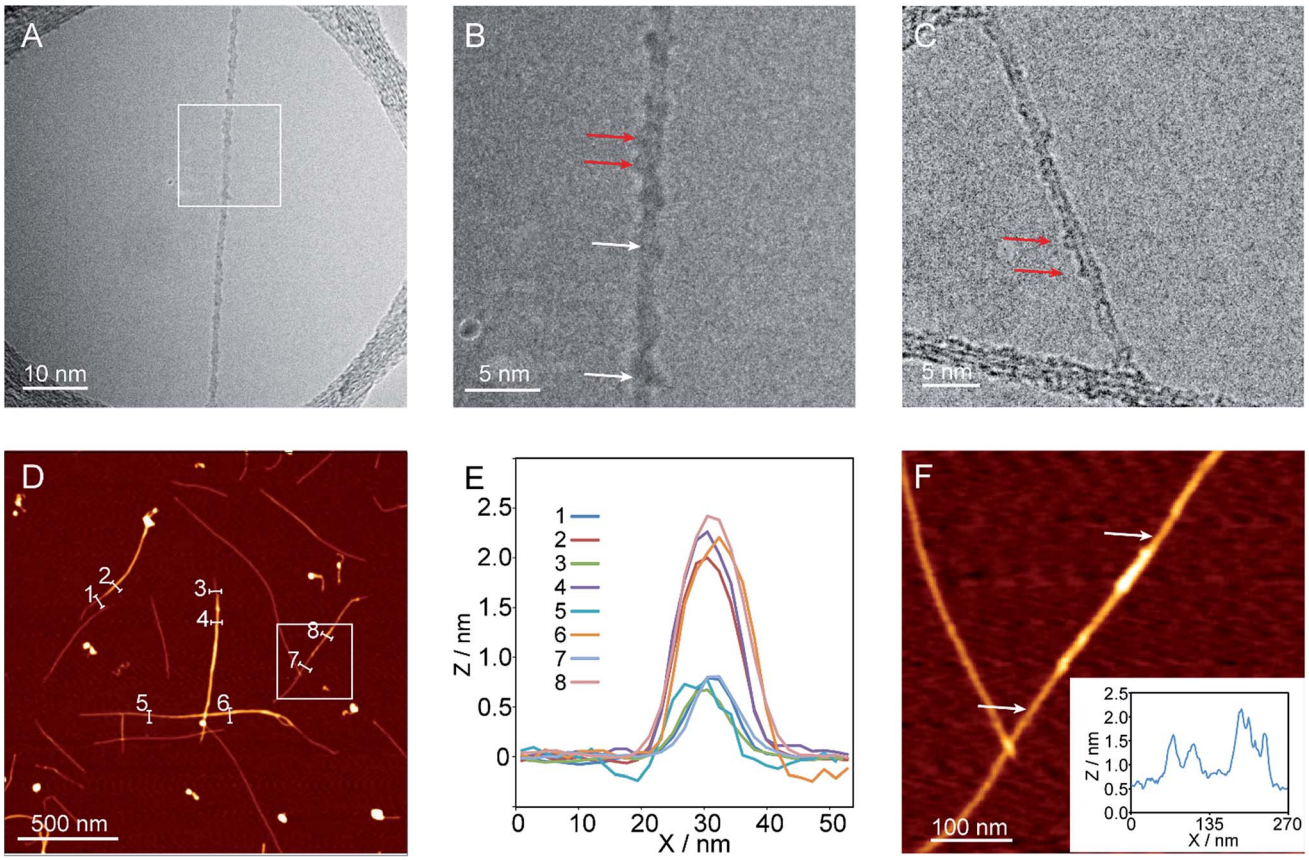

Fig. 5 (A–C) TEM micrographs of the product of the reaction of (6,5)-SWNTs with **3** in DMF. (D) Large-area AFM micrograph of the product of the reaction of (6,5)-SWNTs with **3** in DMF. (E) Height profiles along the lines marked in (D). (F) Zoom-in on the area marked with a white square in (D), showing two individual macrocycles, and a region that could be oligomer-wrapped. The inset shows the height profile between the points marked with white arrows from left to right.

MINTs and oligomer-wrapped SWNTs. Are these structural differences reflected in altered spectroscopic features? Indeed, we found significant differences in the Raman spectra of the products obtained from the metathesis reactions in TCE and DMF. The results of an average of at least three spectra for each product for linear precursor **3** under 532, 633, and 785 nm excitation are summarized in Table 2.

The lack of a consistent increase in the I_D/I_G ratio, together with the clearly visible RBMs (Fig. 6), indicates that the products are not functionalized covalently in any case,[46] as expected for the metathesis reaction conditions. Compared to the pristine nanotubes, the samples run in TCE show larger differences in their G band Raman shift than those from reactions carried out in DMF, even though their degree of functionalization is significantly smaller. For instance, under 532 nm excitation, all products show a small downshift of the G band, indicative of the absence of significant charge-transfer from the nanotubes to the acceptor NDI unit under these conditions. Quantitatively, the shifts for the products from reactions run in TCE and DMF are on average -3 cm^{-1} and -1 cm^{-1}, respectively. The difference between the products obtained in each solvent becomes clearer under red and near-infrared irradiation, where there is a marked upshift of the G band (9–12 cm^{-1}) for the products of the TCE reaction, consistent with significant charge transfer from the SWNTs to the NDI units. In contrast, the products of the reactions run in DMF show much smaller shifts (2–8 cm^{-1}). For instance, in the case of **3**–(7,6) under 633 nm excitation the G^+ band appears at 1580 cm^{-1} for the pristine SWNTs, at 1590 cm^{-1} for **3**–(7,6)-TCE and at 1583 cm^{-1} for **3**–(7,6)-DMF (Fig. 6). These results confirm a less efficient SWNT–NDI interaction in the case of the DMF compared to the TCE products, despite the larger degree of functionalization.

Table 2 Summary of most relevant Raman data for samples of the reactions between linear precursor **3** and both types of SWNTs in TCE and DMF

	λ_{exc} = 532 nm		λ_{exc} = 633 nm		λ_{exc} = 785 nm	
Sample	I_D/I_G	G^+ shift (cm^{-1})	I_D/I_G	G^+ shift (cm^{-1})	I_D/I_G	G^+ shift (cm^{-1})
(6,5) SWNTs	0.06	1576	0.07	1580	0.07	1576
3–(6,5) TCE	0.06	1573	0.07	1589	0.07	1585
3–(6,5) DMF	0.01	1574	0.13	1588	0.23	1579
(7,6) SWNTs	0.07	1570	0.05	1580	0.02	1576
3–(7,6) TCE	0.05	1567	0.07	1590	0.09	1588
3–(7,6) DMF	0.07	1570	0.07	1583	0.09	1584

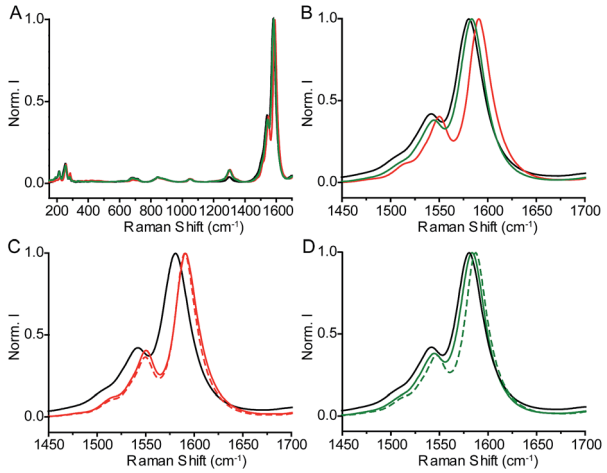

Fig. 6 Raman spectra (λ_{exc} = 633 nm) of (A) (7,6) SWNTs (black line), reaction product of **3** with (7,6) SWNTs in TCE (red line) and in DMF (green line). (B) Zoom-in of the G band of the spectra shown in (A). (C) Partial Raman spectra of (7,6) SWNTs (black line) and the reaction product of **3** with (7,6) SWNTs in TCE before (solid red line) and after (dashed red line) reflux in TCE. (D) Partial Raman spectra of (7,6) SWNTs (black line) and the reaction product of **3** with (7,6) SWNTs in DMF before (solid green line) and after (dashed green line) reflux in TCE.

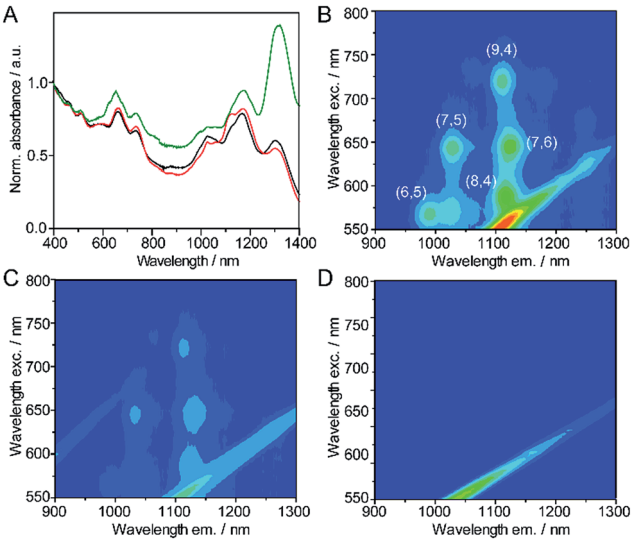

Fig. 7 (A) UV-vis-NIR absorption spectra of pristine (7,6)-enriched SWNTs (black), and the products of their reactions with **3** in TCE (red) and DMF (green). (B) PLE spectrum of pristine (7,6)-enriched SWNTs and the products of their reactions with **3** in TCE (C) and DMF (D). All spectra in D_2O with 1% sodium dodecylsulfate as surfactant and acquired at room temperature. Scattering has not been filtered.

Remarkably, after the thermal treatment, the TCE samples show basically no change in their Raman spectra, whereas those from reactions carried out in DMF suffer larger shifts with respect to the pristine SWNTs, approximating those of the TCE samples. For example, for **3**–(7,6)-DMF, the G^+ band shifts from 1583 cm^{-1} to 1587 cm^{-1}, compared to 1590 cm^{-1} for **3**–(7,6)-TCE (Fig. 6). These changes are in agreement with MINTs becoming predominant in the DMF samples after the thermal treatment.

The absorption and photoemission spectroscopy of the samples also reflects the type of functionalization. Fig. 7A depicts the UV-vis-NIR absorption spectra of pristine (7,6)-enriched SWNTs (black), and the products of their reactions with **3** in TCE (red) and DMF (green).

The SWNTs show absorption features in the S22 and S11† regions of the spectra corresponding to various chiralities, with the (7,6) features at approximately 660 nm and 1120 nm being particularly prominent.[47] Upon functionalization in TCE, we observe small red shifts of all bands in analogy with our previous results for MINTs.[25,26,28] The absorption features of the sample treated in DMF are remarkably different. The relative intensity of the absorption at 1310 nm, which we tentatively assign to either (13,2) or (9,7) SWNTs,[47] increases significantly, most likely due to improved solubility due to functionalization. Since such SWNTs have diameters of around 1.1 nm, and are way too large to undergo MINT formation (see Fig. 2B), we assume they must be oligomer-wrapped.

The 3D photoluminescence excitation (PLE) maps shown in Fig. 7B–D provide more information. The pristine SWNTs show emissions corresponding to (6,5), (7,5), (8,4), (9,4) and (7,6) SWNTs. Upon functionalization in TCE, the luminescence of the smaller (6,5) SWNTs is nearly completely quenched, the (7,5) SWNTs also suffer strong quenching, but are still visible, and the larger nanotubes are quenched to a lesser extent. In contrast, the nanotubes functionalized in DMF show no photoluminescence irrespective of their chirality, and despite being well dispersed according to their absorption spectra. Although luminescence quenching is a complex phenomenon and quantitative conclusions cannot be extracted, our observations point to a chirality-dependent functionalization in TCE and to a nonselective functionalization in DMF, in line with the MM calculations and TGA data.

Fig. 8A shows the changes to the C 1s region of the X-ray Photoelectron Spectra (XPS) upon functionalization of the (7,6) SWNTs with **3**. The pristine sample is intrinsically asymmetric and its main component, related to the primary graphitic peak of carbon or sp^2, is represented by a Doniach-Sunjic function with an asymmetry parameter α = 0.18 and centered in a binding energy of 284.4 eV. The asymmetry of this component is associated with the many-electron response to the sudden creation of a photohole.[48] The rest of the peaks can be perfectly reproduced by Gaussians, as with the typical plasmon loss centered at 290.8 eV and the sp^3 or amorphous carbon at 285.3 eV, visible even in the pristine sample as a result of the hybridization of the sp^2 component.

After treatment with **3**, new features appear in the spectra. Centered at 286.1 eV and at 285.9 eV there is a component that can be assigned to C–N bonds and/or C–O bonds. In agreement with the small degree of functionalization, N is hardly detected for the TCE sample, so the peak at 286.1 eV can be safely assigned to C–O species, which are more abundant in **3**. In the DMF case, this peak is centered at a slightly smaller energy (285.9 eV), and we assume both C–O and C–N functional groups are contributing. To complete the fit it was necessary to add another component at 289.1 eV for the TCE and 288.4 eV for

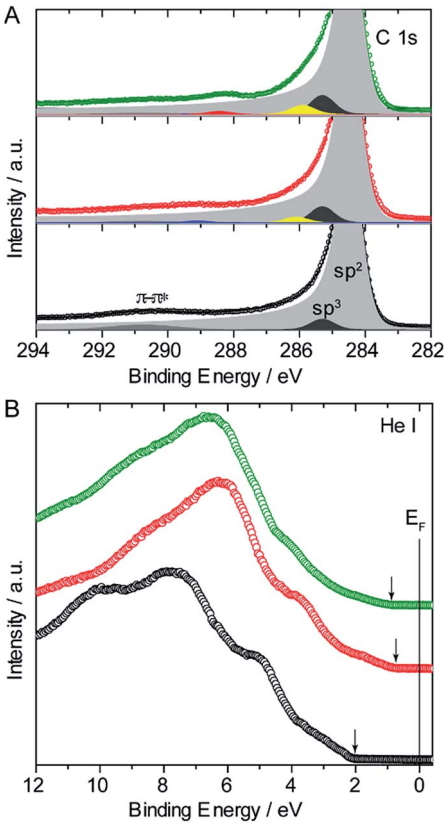

Fig. 8 (A) XPS spectra of C 1s core level for the pristine SWNTs (lower panel, black circles and line), functionalized with **3** in TCE (middle panel, red circles and line) and in DMF (upper panel, green circles and line). Circles are experimental data and the lines represent the fits. (B) UPS spectra measured with He I line of the pristine SWNTs (black circles), functionalized with **3** in TCE (red circles) and in DMF (green circles).

DMF, related to O–C=C and C=O, respectively. Interestingly, all features related to the NDI functionalization show noticeable shifts depending on the solvent used for the reaction.

To study the changes in the valence band with the different functionalization protocols, UPS spectra were also acquired. Fig. 8B shows the valence band of the pristine (7,6) sample (black circles), where most of its features are typical of semiconducting SWNTs, which are in turn directly related to those of graphite: the 2p–σ states around 5 and 8 eV below the Fermi level and the mixed σ–π hybridized states around 10 eV, that come from the curvature of the SWNT.[49,50]

However, in the pristine sample, the 2p–π band located at 3 eV expected for graphite, is not evident here due to the proximity of the border of the valence band at 2 eV, far away from the Fermi level, which gives the semiconductor character to the SWNTs. After reaction with **3** in TCE (red circles) and DMF (green circles) the valence bands show in both cases the typical oxygen band around 6 eV and a significant approach of the border of the valence bands towards the Fermi level (see vertical arrows in Fig. 8B). In line with the Raman results, this effect is more marked for the samples functionalized in TCE, despite the smaller degree of functionalization.

Conclusions

In conclusion, we have described a novel method for the non-covalent functionalization of SWNTs. We used NDI-based bisalkene precursors that can either ring-close around the SWNTs to form rotaxane-like MINTs or oligomerize through ADMP and then wrap the SWNTs. By varying the solvent system we can control the final outcome of the reaction. In TCE, the NDI precursors show lower affinity for the SWNTs, and the non-templated metathesis reaction is very slow. The combination of these two factors favours the formation of the more stable MINTs. In contrast, in DMF, the non-templated reaction is significantly faster, and the NDI precursors show much larger binding constants towards SWNTs, which results in the formation of a substantial amount of oligomer-wrapped SWNTs.

The formation of MINTs in TCE depends on the match between the cavity of the macrocycle(s) and the diameter of the SWNTs. Meanwhile, the degree of functionalization in the reactions run in DMF is fundamentally diameter-independent and consistently leads to larger NDI loading. Each type of functionalization affects the electronic properties of the SWNTs differently, which is reflected in changes in their Raman, UV-vis-NIR, PLE, XPS and UPS spectra.

Our results illustrate how the combination of covalent and noncovalent chemistries opens the door to novel types of functionalization of SWNTs in which the degree of functionalization, the electronic interaction between the nanotubes and their supramolecular partners, and, most remarkably, their topology[51] can be varied.

Acknowledgements

S. L. and E. M. P. gratefully acknowledge funding from the European Research Council MINT (ERC-StG-2012-307609), the MINECO of Spain (CTQ2014-60541-P) and the Comunidad de Madrid (MAD2D project, S2013/MIT-3007). Y. P. and A. R. acknowledge financial support from the European Research Council (ERC-2010-AdG-267374), Spanish grant (FIS2013-46159-C3-1 P), Grupos Consolidados (IT578-13), and AFOSR Grant No. FA2386-15-1-0006 AOARD 144088 H2020-NMP-2014 project MOSTOPHOS, GA no. SEP-210187476 and COST Action MP1306 (EUSpec), as well as technical and human support provided by IZO-SGI SGIker of UPV/EHU and its European funding (ERDF and ESF).

References

1 S. Iijima and T. Ichihashi, *Nature*, 1993, **363**, 603–605.
2 D. S. Bethune, C. H. Kiang, M. S. de Vries, G. Gorman, R. Savoy, J. Vazquez and R. Beyers, *Nature*, 1993, **363**, 605–607.
3 J. M. Schnorr and T. M. Swager, *Chem. Mater.*, 2011, **23**, 646–657.
4 M. F. L. De Volder, S. H. Tawfick, R. H. Baughman and A. J. Hart, *Science*, 2013, **339**, 535–539.

5 Y. Cao, Y. Che, J.-W. T. Seo, H. Gui, M. C. Hersam and C. Zhou, *Appl. Phys. Lett.*, 2016, **108**, 233105.
6 J. G. Weis, J. B. Ravnsbaek, K. A. Mirica and T. M. Swager, *ACS Sens.*, 2016, **1**, 115–119.
7 S. Ishihara, J. M. Azzarelli, M. Krikorian and T. M. Swager, *J. Am. Chem. Soc.*, 2016, **138**, 8221–8227.
8 Q. Cao, S.-J. Han, J. Tersoff, A. D. Franklin, Y. Zhu, Z. Zhang, G. S. Tulevski, J. Tang and W. Haensch, *Science*, 2015, **350**, 68–72.
9 W. Qin, M. Gong, X. Chen, T. A. Shastry, R. Sakidja, G. Yuan, M. C. Hersam, M. Wuttig and S. Ren, *Adv. Mater.*, 2015, **27**, 734–739.
10 S. F. Liu, A. R. Petty, G. T. Sazama and T. M. Swager, *Angew. Chem., Int. Ed.*, 2015, **54**, 6554–6557.
11 P. Singh, S. Campidelli, S. Giordani, D. Bonifazi, A. Bianco and M. Prato, *Chem. Soc. Rev.*, 2009, **38**, 2214–2230.
12 E. Bekyarova, S. Sarkar, F. Wang, M. E. Itkis, I. Kalinina, X. Tian and R. C. Haddon, *Acc. Chem. Res.*, 2013, **46**, 65–76.
13 Y.-L. Zhao and J. F. Stoddart, *Acc. Chem. Res.*, 2009, **42**, 1161–1171.
14 K. Dirian, M. A. Herranz, G. Katsukis, J. Malig, L. Rodríguez-Pérez, C. Romero-Nieto, V. Strauss, N. Martín and D. M. Guldi, *Chem. Sci.*, 2013, **4**, 4335–4353.
15 S. Marchesan, M. Melchionna and M. Prato, *ACS Nano*, 2015, **9**, 9441–9450.
16 H. Kwon, A. o. Furmanchuk, M. Kim, B. Meany, Y. Guo, G. C. Schatz and Y. H. Wang, *J. Am. Chem. Soc.*, 2016, **138**, 6878–6885.
17 M. Barrejon, H. B. Gobeze, M. J. Gomez-Escalonilla, J. L. G. Fierro, M. Zhang, M. Yudasaka, S. Iijima, F. D'Souza and F. Langa, *Nanoscale*, 2016, **8**, 14716–14724.
18 J. Chen, J. H. Walther and P. Koumoutsakos, *Adv. Funct. Mater.*, 2015, **25**, 7539–7545.
19 I. Pochorovski, H. Wang, J. I. Feldblyum, X. Zhang, A. L. Antaris and Z. Bao, *J. Am. Chem. Soc.*, 2015, **137**, 4328–4331.
20 A. Feng, L. Peng, B. Liu, S. Liu, S. Wang and J. Yuan, *ACS Appl. Mater. Interfaces*, 2016, **8**, 11024–11030.
21 M. Mollahosseini, E. Karunaratne, G. N. Gibson, J. A. Gascon and F. Papadimitrakopoulos, *J. Am. Chem. Soc.*, 2016, **138**, 5904–5915.
22 G. Clavé, G. Delport, C. Roquelet, J.-S. Lauret, E. Deleporte, F. Vialla, B. Langlois, R. Parret, C. Voisin, P. Roussignol, B. Jousselme, A. Gloter, O. Stephan, A. Filoramo, V. Derycke and S. Campidelli, *Chem. Mater.*, 2013, **25**, 2700–2707.
23 I. Hijazi, T. Bourgeteau, R. Cornut, A. Morozan, A. Filoramo, J. Leroy, V. Derycke, B. Jousselme and S. Campidelli, *J. Am. Chem. Soc.*, 2014, **136**, 6348–6354.
24 T. Lei, X. Chen, G. Pitner, H. S. P. Wong and Z. Bao, *J. Am. Chem. Soc.*, 2016, **138**, 802–805.
25 A. de Juan, Y. Pouillon, L. Ruiz-González, A. Torres-Pardo, S. Casado, N. Martín, A. Rubio and E. M. Pérez, *Angew. Chem., Int. Ed.*, 2014, **53**, 5394–5400.
26 A. López-Moreno and E. M. Pérez, *Chem. Commun.*, 2015, **51**, 5421–5424.
27 A. de Juan, M. Mar Bernal and E. M. Pérez, *ChemPlusChem*, 2015, **80**, 1153–1157.
28 E. Martínez-Periñán, A. de Juan, Y. Pouillon, C. Schierl, V. Strauss, N. Martín, A. Rubio, D. M. Guldi, E. Lorenzo and E. M. Pérez, *Nanoscale*, 2016, **8**, 9254–9264.
29 Rotaxanes and pseudorotaxanes are both topologically trivial and, mathematically speaking, neither is mechanically interlocked, since they can be converted into the macrocycle-dumbell or macrocycle-thread pairs by shrinking the stoppers and/or stretching out the macrocycle to allow dissociation. From a chemical perspective, this would require that the species withstand the shrinking or stretching without breaking a covalent bond. This, we believe, is a more adequate criterion than the presence or absence of stoppers to decide if the species are mechanically interlocked or not (see: A. de Juan and E. M. Pérez, *Nanoscale*, 2013, **5**, 7141). Since MINTs require breaking of covalent bonds to dissociate, we consider them mechanically interlocked.
30 S. V. Bhosale, C. H. Jani and S. J. Langford, *Chem. Soc. Rev.*, 2008, **37**, 331–342.
31 X. Zhan, A. Facchetti, S. Barlow, T. J. Marks, M. A. Ratner, M. R. Wasielewski and S. R. Marder, *Adv. Mater.*, 2011, **23**, 268–284.
32 H. E. Katz, A. J. Lovinger, J. Johnson, C. Kloc, T. Siegrist, W. Li, Y. Y. Lin and A. Dodabalapur, *Nature*, 2000, **404**, 478–481.
33 M. Sommer, *J. Mater. Chem. C*, 2014, **2**, 3088–3098.
34 R. Kim, P. S. K. Amegadze, I. Kang, H.-J. Yun, Y.-Y. Noh, S.-K. Kwon and Y.-H. Kim, *Adv. Funct. Mater.*, 2013, **23**, 5719–5727.
35 V. Senkovskyy, R. Tkachov, H. Komber, M. Sommer, M. Heuken, B. Voit, W. T. S. Huck, V. Kataev, A. Petr and A. Kiriy, *J. Am. Chem. Soc.*, 2011, **133**, 19966–19970.
36 S. L. Suraru and F. Wurthner, *Angew. Chem., Int. Ed.*, 2014, **53**, 7428–7448.
37 P. Ballester, *Acc. Chem. Res.*, 2012, **46**, 874–884.
38 S. Guha, F. S. Goodson, L. J. Corson and S. Saha, *J. Am. Chem. Soc.*, 2012, **134**, 13679–13691.
39 S. Guha and S. Saha, *J. Am. Chem. Soc.*, 2010, **132**, 17674–17677.
40 V. Gorteau, G. Bollot, J. Mareda, A. Pérez-Velasco and S. Matile, *J. Am. Chem. Soc.*, 2006, **128**, 14788–14789.
41 N. Ponnuswamy, G. D. Pantos, M. M. J. Smulders and J. K. M. Sanders, *J. Am. Chem. Soc.*, 2012, **134**, 566–573.
42 A. R. Stefankiewicz, E. Tamanini, G. D. Pantos and J. K. M. Sanders, *Angew. Chem., Int. Ed.*, 2011, **50**, 5725–5728.
43 Z. Hu, G. D. Pantos, N. Kuganathan, R. L. Arrowsmith, R. M. J. Jacobs, G. Kociok-Koehn, J. O'Byrne, K. Jurkschat, P. Burgos, R. M. Tyrrell, S. W. Botchway, J. K. M. Sanders and S. I. Pascu, *Adv. Funct. Mater.*, 2012, **22**, 503–518.
44 E. M. Pérez and N. Martín, *Chem. Soc. Rev.*, 2008, **37**, 1512–1519.
45 Our method is based on the direct measurement of the concentration of bound and free host molecules in the equilibrium, so that the "concentration" of SWNTs does not need to be known. See: A. de Juan, A. López-Moreno, J. Calbo, E. Ortí and E. M. Pérez, *Chem. Sci.*, 2015, **6**, 7008–7014.

46 C. Fantini, M. L. Usrey and M. S. Strano, *J. Phys. Chem. C*, 2007, **111**, 17941–17946.
47 S. M. Bachilo, M. S. Strano, C. Kittrell, R. H. Hauge, R. E. Smalley and R. B. Weisman, *Science*, 2002, **298**, 2361–2366.
48 S. Hüfner, *Photoelectron Spectroscopy. Principles and Applications*, Springer, Berlin Heidelberg, 3rd edn., 2003.
49 P. Chen, X. Wu, X. Sun, J. Lin, W. Ji and K. L. Tan, *Phys. Rev. Lett.*, 1999, **82**, 2548–2551.
50 M. Scardamaglia, C. Struzzi, F. J. Aparicio Rebollo, P. De Marco, P. R. Mudimela, J.-F. Colomer, M. Amati, L. Gregoratti, L. Petaccia, R. Snyders and C. Bittencourt, *Carbon*, 2015, **83**, 118–127.
51 We have recently shown that changes in the topology of SWNT noncovalent derivatives affect their properties dramatically, see: A. López-Moreno, B. Nieto-Ortega, M. Moffa, A. de Juan, M. M. Bernal, J. P. Fernández-Blázquez, J. J. Vilatela, D. Pisignano and E. M. Pérez, *ACS Nano*, 2016, **10**, 8012–8018.